



HAL
open science

Magnetic Field Changes Macrophage Phenotype

Jarek Wosik, Wei Chen, Kuang Qin, Rafik M Ghobrial, Jacek Z Kubiak,
Malgorzata Kloc

► **To cite this version:**

Jarek Wosik, Wei Chen, Kuang Qin, Rafik M Ghobrial, Jacek Z Kubiak, et al.. Magnetic Field Changes Macrophage Phenotype. *Biophysical Journal*, 2018, 114 (8), pp.2001-2013. 10.1016/j.bpj.2018.03.002 . hal-01780368v1

HAL Id: hal-01780368

<https://univ-rennes.hal.science/hal-01780368v1>

Submitted on 9 Jul 2018 (v1), last revised 6 Sep 2018 (v2)

HAL is a multi-disciplinary open access archive for the deposit and dissemination of scientific research documents, whether they are published or not. The documents may come from teaching and research institutions in France or abroad, or from public or private research centers.

L'archive ouverte pluridisciplinaire **HAL**, est destinée au dépôt et à la diffusion de documents scientifiques de niveau recherche, publiés ou non, émanant des établissements d'enseignement et de recherche français ou étrangers, des laboratoires publics ou privés.

1
2
3
4
5
6
7
8
9
10
11
12
13
14
15
16
17
18
19
20
21
22
23
24

Magnetic field changes macrophage phenotype

J. Wosik^{*1,2}, *W.Chen*^{3,4}, *K. Qin*^{1,2}, *R M. Ghobrial*^{3,5}, *J. Z. Kubiak*^{6, 7, 8},
M.Kloc^{*3, 5,9}

Short title: macrophages on magnet

Corresponding Author

M.Kloc
or

J. Wosik

1 Electrical and Computer Engineering Department, University of Houston, Houston, Texas

2 Texas Center for Superconductivity, University of Houston, Houston, Texas

3 The Houston Methodist Research Institute, Houston, Texas

4 Department of Nephrology, Second Xiangya Hospital, Central South University, Changsha, China

5 Department of Surgery, The Houston Methodist Hospital, Houston, Texas

6 Univ Rennes, CNRS, IGDR (Institute of Genetics and Development of Rennes), UMR 6290, Cell Cycle Group, Faculty of Medicine, Rennes, France

7 Department of Regenerative Medicine, Military Institute of Hygiene and Epidemiology (WIHE), Warsaw, Poland

8 Department of Genetics, The University of Texas, M.D. Anderson Cancer Center, Houston, Texas

25 **Abstract**

26 Macrophages play a crucial role in homeostasis, regeneration, and innate and adaptive immune
27 response. Functionally different macrophages have different shape and molecular phenotype that
28 depend on actin cytoskeleton, which is regulated by small GTPase RhoA. The naive M0
29 macrophages are slightly elongated, pro-inflammatory M1 are round and M2 anti-inflammatory
30 macrophages are elongated. We have recently shown in the rodent model system that genetic
31 or pharmacologic interference with the RhoA pathway deregulates macrophage actin
32 cytoskeleton, causes extreme macrophage elongation and prevents macrophage migration.
33 Here we report that an exposure of macrophages to a nonuniform magnetic field causes extreme
34 elongation of macrophages and has a profound effect on their molecular components and
35 organelles. Using immunostaining and Western blotting, we observed that magnetic force
36 rearranges the macrophage actin cytoskeleton, Golgi complex and cation channel receptor
37 TRPM2 and modifies expression of macrophage molecular markers. We have found that the
38 magnetic field-induced alterations are very similar to changes caused by RhoA interference. We
39 also analyzed magnetic field-induced forces acting on macrophages and found that the location
40 and alignment of magnetic-field-elongated macrophages correlate very well with the
41 simulated distribution and orientation of such magnetic-force lines.

42

43 **Keywords:** macrophages, magnetic field, RhoA knockout, cytoskeleton, chronic rejection,
44 mechanotransduction, magnetic force

45

46

47

48

49

50

51 **INTRODUCTION**

52 Macrophages have several functionally different phenotypes/subtypes. M0 macrophages are
53 naïve/unpolarized macrophages. One of the most common subtypes of activated macrophages
54 are M1 proinflammatory “killer” macrophages, which produce damaging reactive oxygen
55 species and express nitric oxide synthase iNOS, and M2 anti-inflammatory “repair”
56 macrophages, which produce enzyme Arginase-1 that depletes L-arginine and deprives iNOS of
57 its substrate (4-7).

58 Macrophages, like all eukaryotic cells, contain an actin-filament cytoskeleton. Macrophage
59 migration occurs via dynamic rearrangements of actin filaments. Our recent studies showed
60 that pharmacologic or genetic interference with the small GTPase RhoA pathway, which
61 is the master regulator of actin, causes extreme elongation of macrophages (hummingbird
62 phenotype), disrupts the Golgi/endosomal pathway, prevents macrophage migration into the
63 graft (through the clustering of the CX3CR1 receptor) and inhibits chronic rejection in the
64 rodent model system (4-7).

65 Here we were interested in finding out if an external magnetic field, in conjunction with
66 transduction processes, could induce cytoskeletal rearrangements in macrophages and change
67 their shape and molecular and organellar phenotype.

68 It is already known that external mechanical force applied to the cell has a direct impact and
69 can affect the cell cytoskeleton (8, 9). It is also known that nonuniform magnetic fields can
70 create such magnetic force-driven stimuli. The cell responds to the external stimuli by
71 remodeling the cytoskeleton, which is visco-elastic and provides a continuous mechanical
72 coupling throughout the cell as it changes. This, in turn, induces an internal cell stress and
73 changes in certain cellular components and components such as actin-filament polymerization,

74 focal adhesions, etc. Such conversion of mechanical forces to biochemical interactions is referred
75 to as mechanotransduction. There are reports that changes in ion-channel activity at the plasma
76 membrane of cells may convey mechanical stresses from the cell membrane to internal
77 organelles, causing changes in gene transcription and inducing apoptosis (10). Other reports
78 show that pathways of mechanically induced cell damage can include activation of the Caspase-3
79 protease pathway (11) and TNF-related apoptosis-inducing ligand (TRAIL/Apo2L) (12) and also
80 cleavage of Caspases 3 and 9 (13).

81 In spite of outstanding recent progress in research of the influence of electromagnetic fields on
82 the biology of cells and the expanding use of magnetic materials in biomedical applications,
83 surprisingly little is known about the influence of a magnetic field at the cellular level (14, 15).
84 The nature and strength of interactions of electromagnetic fields with cell or tissue mainly
85 depend on electric- and magnetic-field-produced polarizations. The ability to induce such
86 polarizations is measured by electric and magnetic-field susceptibilities. There are significant
87 differences between interactions of both fields with cells/tissue, because for a typical tissue the
88 electric susceptibility is 10^5 - 10^6 times larger than the magnetic-field susceptibility and, as a
89 result, the presence of the electric field can cause significant cell/tissue damage, whereas
90 magnetic-field interactions with cell/tissue are relatively weak.

91 There are mixed reports about the influence of magnetic fields on cell growth and functions,
92 and most but not all studies suggest that there is no obvious observable effect, even at as high as
93 10 T or higher values of uniform magnetic fields. In addition, although such fields in some
94 studies have been shown to affect cell differentiation and viability; they did not have long-
95 lasting, damaging effects (16). Furthermore, the nonuniform magnetic fields, in contrast to the
96 uniform fields, were proven to generate sufficiently large magnetically induced mechanical

97 forces able to affect cell morphology, differentiation and functionality (17, 18). As a result a few
98 in vitro studies carried out recently for spatially modulated magnetic fields showed a clear
99 magnetic field-cell interaction (19-21). Although there are many technical challenges to generate
100 sufficiently high fields and gradients, recent progress in fabrication of strong permanent magnets
101 based on rare-earth elements and also use of patterned magnetic microstructures have allowed
102 generation of highly nonuniform magnetic fields, resulting in local gradients' magnitudes
103 reaching up to extremely high, such as 10^6 -T/m, values (22).

104 In these studies, we have designed a permanent rare-earth magnet setup with well-defined
105 magnetic fields and field-gradient patterns; and we have investigated the effect of these fields
106 and results from the presence of magnetic force on cultured, unpolarized/naïve mouse peritoneal
107 macrophages.

108 **MATERIAL AND METHODS**

109 **Magnetic field/field-gradients generation**

110 Experiments with cultured macrophages were carried out, using a pair of permanent
111 neodymium-iron-boron (NdFeB) flat planar magnets to generate the desired magnetic-field
112 patterns. The magnets' dimensions were 5 mm by 10 mm by 1.9 mm, and they were zinc-plated
113 and axially magnetized in a direction perpendicular to the 5-mm by 10-mm plane (Digi-Key,
114 ND105236). Two combinations of the magnetization direction were selected for the planar
115 alignment of two identical magnets: a parallel NS-NS and anti-parallel NS-SN configuration.
116 The adjacent surfaces of the magnets were highly polished and, by using custom-made
117 nonmagnetic tools, they were framed together with no gaps left between their surfaces. The
118 magnets used in experiments had the following parameters: remanence magnetization B_r (min)
119 1.24 T, coercivity H_{cB} (induction curve) 950 kA/m, and coercivity H_{cJ} (polarization curve) 1750

120 kA/m. A fiber-epoxy G-10 material was used to make a holder for the chamber slide containing
121 macrophages in culture medium and generating a magnetic-field NdFeB magnet structure. A 0.1-
122 mm-thick cover glass separated the macrophages from the magnets. A custom-made chamber
123 slide containing macrophages in culture medium was placed atop the NdFeB magnets. The
124 replacement of a 1-mm-thick standard microscope slide with a much thinner (0.1-mm thick)
125 cover glass allowed us to decrease the distance between the magnetic structure and the
126 macrophages, which settle and grow on the bottom surface of the chamber.

127 Magnetic-field simulations of the magnetic field, magnetic-field gradient and magnetic-force
128 distribution were carried out to analyze the forces exerted by the gradient field on the
129 macrophages. All calculations were performed using the magnetic-fields module of COMSOL
130 Multiphysics 5.0, an interactive full-wave, finite element-based software package (23). AC/DC
131 and Mathematics software modules were employed for the calculations. Also, Ansoft (Maxwell)
132 similar numerical method software was used for some simulations. The magnets' geometry,
133 material parameters, and field boundary conditions were selected according to the experimental
134 magnet configuration and used magnetic materials. The magnetization strength of the 2
135 permanent magnets used in experiments was defined through their known remanence and
136 coercivity values. The geometry of the magnets' configuration was modeled so as to be very
137 close to the experimental setup dimensions, as shown in Figures 1 and 2.

138 The magnetic field is calculated in a magnetostatic configuration. The magnetic-field gradient
139 is obtained by taking the derivative of the z-component of the B-field. As the last step, from the
140 formula $\vec{F} = V \Delta \chi (\vec{B} \cdot \nabla \vec{B}) / \mu_0$, the magnetic field was calculated, using the field calculator
141 option in the Maxwell software.

142 To keep magnets as close as possible to the cells, we modified chamber slides, replacing the
143 existing microscope slide with a much thinner microscope cover glass. The 1-well chamber
144 slides were modified as follows: the chamber was detached from the microscope slide, and all
145 silicone was removed. The indented edges of the chamber were coated, using the wooden end of
146 a Q-tip, with Dow Corning high-vacuum grease; and the chamber was firmly attached to the
147 24x60-mm microscope cover glass. The thusly constructed chamber slide was placed in a holder
148 containing magnets (or without magnets present for control purposes) and sterilized with 70%
149 ethanol in a cell-culture hood for 3 days before use. Just before seeding the macrophages, we
150 removed the ethanol and rinsed the chamber slides 3 times with sterile PBS and once with
151 Modified Eagle Medium.

152 **Animals and peritoneal macrophages**

153 Generation of RhoA-deficient $Lyz2^{Cre+/-}$ $RhoA^{flox/flox}$ mice was described previously (6).
154 Breeding and all experiments were performed according to Methodist Hospital Research
155 Institute's animal care protocol and met NIH standards in concordance with the "Guide for the
156 Care and Use of Laboratory Animals" (DHHS publication No. (NIH) 85-23 Revised 1985), the
157 PHS "Policy on Humane Care and Use of Laboratory Animals" and the NIH "Principles for the
158 Utilization and Care of Vertebrate Animals Used in Testing, Research and Training." All studies
159 carried out here were approved by Houston Methodist Institutional Animal Care and Use
160 Committee and animal protocol AUP-0317-0006 (IS00003962), entitled, "Tolerance Induction in
161 a Rodent System" was used. Mice euthanasia was performed according to the TMHRI
162 Euthanasia of Rodents Procedure, by isoflurane overdose via a vaporizer inhalation, followed by
163 cervical dislocation and thoracotomy to ensure death.

164 Peritoneal macrophages were collected in PBS from the peritoneal cavity of euthanized
165 C57BL/6 (wild-type) or RhoA-deficient $Ly2^{Cre+/-}$ $RhoA^{flox/flox}$ (RhoA KO) mice. The collected
166 cell suspension was centrifuged at 1700 RPM for 5 min, supernatant was discarded, and the
167 cells' pellet was resuspended in Dulbecco Modified Eagle Medium supplemented with 10%
168 FBS, 100U/mL penicillin and 100ug/mL streptomycin. The macrophages from C57BL/6 mice
169 were seeded in the magnets' chamber slides. For control, the C57BL/6 macrophages were grown
170 on slides without magnets. The macrophages from RhoA KO mice were seeded only on chamber
171 slides without magnets.

172 After overnight incubation at 37° and 5% CO₂, the medium was replaced with fresh medium.
173 After another overnight incubation, macrophages were fixed in chamber slides.

174 **Fixation, actin, vinculin, Golgi and TRPM2 staining**

175 Macrophages were fixed in chamber slides in 1% formalin in 1 x PBS with 0.05% Triton for
176 30 min at room temperature, washed 3x15 min with PBS-0.05% Tween 20, and blocked
177 overnight at 4°C in Casein blocker in PBS (Biorad) with 0.05% Tween 20. Subsequently,
178 macrophages were incubated with 1:200 dilution of anti-vinculin-FITC conjugated antibody
179 (Sigma, USA), anti-GM130 (Golgi marker) antibody (Biorbyt or Sigma), anti-TRPM2 antibody
180 (ThermoFisher, USA) and rhodamine-phalloidin (Molecular Probes, Eugene, OR; 3 µL of
181 methanolic stock solution of 200 U/mL per 200 µL of blocking buffer) in casein blocking buffer,
182 in the dark, at room temperature for 3 hr. After washing, the GM130- and TRPM2-bound
183 macrophages were incubated with FITC-conjugated secondary antibodies in blocking solution
184 for several hours. Next, macrophages were washed 3 times, 1 hr each, in PBS-0.05% Tween 20,
185 at room temperature, in the dark, mounted in Antifade with Dapi (Molecular Probes) and
186 observed with a (wide-field nonconfocal) Nikon fluorescent microscope.

187 **Western blotting**

188 Macrophages collected from chamber slides were pelleted for 5 min at 3200-rpm
189 centrifugation, resuspended in 1× loading buffer with Halt™ Protease Inhibitor Cocktail and
190 boiled for 5 min. The lysates were resolved on SDS-PAGE and blotted (Trans-Blot® Turbo™)
191 to an LF PVDF membrane. Blots were blocked in 5% fat-free milk in TBST at room temperature
192 for 2 hrs. Subsequently blots were incubated with primary antibodies (GAPDH, Cell Signaling
193 Technology at 1:1000 dilution, Arg-1, R&D systems, at 1:5000 and iNOS, eBioscience, at
194 1:5000 dilution) in blocking solution, overnight at 4°. After washing 3 times (20 min each wash)
195 in TBST, blots were incubated with 1:5000 dilution of secondary antibodies (Goat anti rabbit
196 HRP, Santa Cruz, Rabbit anti-Sheep IgG (H+L) HRP, Invitrogen™, and Goat antirat HRP, Santa
197 Cruz), washed 3 times (20 min each wash) in TBST; and protein bands were visualized on X-ray
198 film, using GAPDH- SuperSignal™ West Pico Chemiluminescent Substrate (Thermo Fisher) or
199 Immobilon Western Chemiluminescent HRP Substrate (EMD Millipore).

200 **RESULTS**

201 **Magnetic-field generation**

202 Two different configurations of each pair of the magnets were used for experiments: NS-NS
203 and NS-SN, where N and S are north and south magnetic poles, respectively. However, results
204 presented in this article, for consistency, were selected only for the NS-SN configuration. In this
205 configuration, due to a much higher gradient above the interface between the 2 magnets, a
206 proportionally stronger influence of the magnetic field compared with the parallel configuration
207 was observed. In Figure 1, 2D simulations of the magnetic field, magnetic-field gradient and
208 magnetic force are shown.

209

210 Calculations were done for the NS-SN configuration, along the y-axis. Simulations presented
211 in Figures 1A, 1B and 1C indicate that, above the interface of the 2 polarized in opposite
212 directions magnets, there is a very steep gradient due to a large change of field magnitude along
213 only a 200-300- μm distance. Also, steep gradients exist on both magnets' edges. A plot of
214 mechanical force acting on the macrophages placed above the magnets is shown in Figure 1D. It
215 can be seen that the force distribution map follows the gradient magnitude change.

216 Figure 2 shows the locations of the most characteristic areas above magnets, where highly
217 elongated and magnetic-field-unaffected macrophages were observed.

218 For the elongated case, 2 such locations were selected, the first above the magnets' interface,
219 where the maximum gradient was created, and the second close to the magnet corners along the
220 diagonal line of the whole structure. In the first and second locations, the longest macrophages
221 and waves of long-range, aligned, elongated macrophages were observed. The calculated
222 distribution of the magnetic field-induced-force component present above the magnets is also
223 marked.

224

225 **Analysis of macrophage phenotype**

226 For our experiments isolated peritoneal M0 macrophages from C57BL/6 mice were seeded on
227 modified chamber slides with the cover glass bottom placed on magnets (see Material and
228 Methods) and grown for 48 hr. For control the C57BL/6 macrophages were grown on slides
229 without magnets. Subsequently, macrophages were fixed; stained for actin, vinculin (focal
230 adhesion marker) and Golgi complex with GM130 protein Golgi marker; and analyzed by
231 fluorescence microscopy. The morphology of macrophages and Golgi and vinculin staining were
232 compared to that of RhoA-deleted macrophages, which were grown without magnets.

233 **Phenotype of macrophages exposed to a magnetic field**

234 When we looked at distribution of actin-stained macrophages on the slides, we found that,
235 while macrophages grown without magnets had uniform distribution on the slide surface (Figure
236 3A, B), the macrophages grown on magnets were aligned in distinct rows or waves and
237 extremely elongated within these rows (Figure 3C, D, E).

238 The calculation of the number of elongated macrophages within 2 mm² areas (from 5 different
239 magnet setups) within the rows shows that there is a statistically significant difference in the
240 number of elongated macrophages counted on the magnet and outside the magnet (Figure 3F).

241 Analysis of macrophage morphology showed that macrophages grown in control chambers
242 without magnets were slightly elongated, with an average length around 50 μm (Figure 3A, B
243 and Figure 4B). In contrast, macrophages grown on magnets had an extremely elongated tail and
244 average length > 150 μm (Figure 3E, F; Figure 4 A, C). A degree of this extreme elongation was
245 very similar to the elongation of the hummingbird phenotype macrophages with deleted RhoA
246 (Figure 4 A, D).

247

248 **Analysis of focal adhesions and Golgi complex in magnetic field-exposed macrophages**

249 We showed previously that the hummingbird phenotype of RhoA-deleted macrophages was
250 caused by inability to disassemble vinculin-rich focal adhesions in the macrophage tail (6). To
251 see if a similar mechanism was responsible for elongation of macrophages grown on magnets,
252 we immunostained them with anti-vinculin antibody.

253

254

255 Figure 5 shows that in control macrophages vinculin-positive staining was concentrated in the
256 macrophage body, around the nucleus and in the area occupied by the podosomes (Figure 5A-C).
257 In magnet-grown macrophages vinculin staining was present in the macrophage body; in the
258 podosome area; and, surprisingly, also in the nuclei (Figure 5 F-I), but in contrast to the RhoA-
259 deleted macrophages (Figure 5 D, E), was absent in the tail (Fig. 5 H, I). Calculation of the
260 number of cells with the nuclear vinculin showed that in magnet-exposed macrophages 95 of the
261 total 136 counted had vinculin present in the nuclei. In contrast, only 2 control macrophages of a
262 total 119 counted had vinculin in the nuclei. The extreme elongation of magnet-grown
263 macrophages and the disruption of their vinculin localization indicate the disruption of the
264 normal actin cytoarchitecture. Because one of the organelles whose organization depends on
265 actin is the Golgi complex, we also stained macrophages with Golgi marker anti-GM130 protein
266 antibody.

267 Golgi staining showed that in control macrophages the Golgi complex was very compact and
268 situated in close vicinity to the nucleus (Figure 6A). In contrast, macrophages grown on magnets
269 showed vesicular GM130 staining in the cytoplasm of the cell body and complete absence of a
270 defined Golgi complex (Figure 6B). In comparison, in the RhoA-deleted macrophages Golgi
271 staining was highly diminished, but some of the staining was still present in the vicinity of the
272 nucleus (Figure 6C).

273 *All these observations indicate that the applied magnetic field had a profound effect on the*
274 *macrophage actin cytoskeleton and actin-dependent molecules and structures, such as vinculin*
275 *(focal adhesions) and the Golgi complex.*

276 **Molecular-marker expression in magnetic field-exposed macrophages**

277 Western blot analysis with anti-iNOS and anti-Arg-1 antibodies, which are the markers of M1
278 and M2 macrophage subtypes, respectively, showed that, while control and magnet-grown M0
279 macrophages did not express the M1 marker iNOS protein, the expression of the M2 marker
280 Arg-1 was highly upregulated in magnet-grown MO macrophages (Figure 7).

281 This indicates that a magnetic field induced both morphological (elongation) and molecular
282 changes in M0 macrophages toward the M2 (anti-inflammatory) phenotype. Although Arg-1 is
283 the signature marker of M2 macrophages, a low level of Arg-1 expression in MO macrophages is
284 quite common because, although these macrophages are theoretically nonactivated, they often
285 show, depending on the mouse state and environment, some degree of activation.

286 **Cation channel distribution**

287 The TRPM2 (the cation channel transient receptor potential melastatin 2/Transient Receptor
288 Potential Cation Channel Subfamily M Member 2) is a Ca^{2+} -permeable cation channel that
289 belongs to the ion transport protein family. Studies in the gastric inflammation mice model
290 showed that TRPM2-deficient macrophages have disrupted Ca^{2+} homeostasis and are unable to
291 control intracellular calcium levels, which results in calcium overloading (25,26). Our
292 preliminary data show that macrophages exposed to magnetic field gradient cluster TRPM2 in
293 the vicinity of the nucleus (Figure 8).

294 Such a clustering may render the channels nonfunctional and disrupt normal Ca^{2+} homeostasis.
295 Because it is known that actin polymerization and organization are Ca^{2+} - dependent, such a
296 disruption may cause changes in the macrophage actin cytoskeleton and actin-related functions.

297 In summary, we showed that the exposure of macrophages to the magnetic field causes
298 macrophage elongation and disrupts actin-dependent molecules and structures, such as the Golgi

299 complex, vinculin (focal adhesions) and receptors. These changes mimic the changes caused by
300 macrophage-specific deletion of RhoA (Figure 9).

301 **DISCUSSION**

302 Two possible forces acting on macrophages can be defined: (i) the Lorentz force, as sketched
303 in Figure 10A, and (ii) the susceptibility buoyance volume force (from Archimedes' principle)
304 acting on a cell suspended in a buffer medium and subjected to a nonuniform magnetic field, as
305 is shown in Figure 10B.

306 The Lorentz force will be created due to the magnetic-field interaction with ionic currents in
307 the membrane. Such force will be present in both uniform and nonuniform (inhomogeneous)
308 fields. There are reports about the influence of static magnetic fields on cells where modified cell
309 shape, structural changes in plasma membrane and increased level of intracellular Ca^{2+} have
310 been observed. One example of such changes was reported by Chionni *et al.*, (27) where
311 lymphocytes and U937 cells in the presence or absence of apoptosis-inducing drugs were
312 strongly affected by the presence of a static magnetic field.

313 The second force leading to interaction of a static magnetic field with cells is caused by the
314 difference between physical characteristics between cells and the cell medium. From
315 Archimedes' principle in the presence of a magnetic -field gradient, there will be force acting on
316 cells. The magnetic energy experienced by a cell placed in a magnetic field can be written as

$$317 \quad U = -\frac{\vec{m}\vec{B}}{2}, \quad (1)$$

318 where $\vec{m} = \chi V \vec{B} / \mu_0$ is the dipole moment, with χ and V representing the susceptibility and
319 volume of the cell, respectively, and μ_0 being the permeability of free space equal to $4\pi \times 10^7$
320 H/m. Since the volume of a biological cell is relatively small, we assume that the magnetic field

321 and susceptibility are constant over the cell volume. Rewriting the magnetic energy equation as
322 $U = VC B^2 / 2\mu_0$, and using the magnetic-force equation, defined as $\vec{F}(x,y,z) = \nabla U$, results in the
323 following formula:

$$324 \quad \vec{F}(x,y,z) = \frac{V(\chi_M - \chi_c)}{\mu_0} \vec{B} \cdot (\nabla \vec{B}) \quad (2)$$

325 As can be seen from this equation, the magnetic force is dependent on the product of the
326 magnetic induction \vec{B} (in T units) with the magnetic-field gradient $\nabla \vec{B}$ (in T/m). Since it is
327 directly proportional to the product of the two, it is often referred to as the “force product”; and it
328 is given in T²/m units. This force is a result of magnetic buoyancy and the diamagnetic repulsive
329 forces. The close-to-interface gradient magnitude is estimated as 10⁴ T/m, and it is relatively
330 large, but smaller than gradients achieved for periodically patterned structures (19, 24, 28).

331 The nature and strength of interactions of electromagnetic fields with cell or tissue mainly
332 depend on electric- and magnetic-field-produced polarizations. The ability to induce such
333 polarizations is measured by electric and magnetic-field susceptibilities. There are significant
334 differences between interactions of both fields with cells/tissue, because for a typical tissue the
335 electric susceptibility is 10⁵-10⁶ times larger than the magnetic-field susceptibility; and, as a
336 result, the electric-field presence can cause significant cell/tissue damage, whereas magnetic
337 field interactions with cell/tissue are relatively weak. Cells are mostly diamagnetic and, in
338 principle, when suspended in a nonmagnetic medium, they are expelled by the magnetic field.
339 However, buffer medium can be either dia- or paramagnetic; and in such a case the response of
340 cells to the presence of a magnetic field (20, 29) mainly depends on the difference between
341 susceptibilities of the cell and medium. Most biological cells are weakly diamagnetic. The force
342 direction will depend on the sign of the magnetic susceptibility difference $\Delta\chi$. For positive $\Delta\chi$,

343 cells will be attracted to the highest gradient lines; whereas for the negative sign, repulsion will
344 take place. Our experiments showed that cells are attracted to the highest gradient line (as
345 defined in Figure 10), clearly indicating that macrophages are more diamagnetic than medium.
346 In Figure 11 we present a plot of the magnetic force calculated for two reverse-polarized (NS-
347 SN) magnets as a function of the x, y position. A good correlation between the calculated
348 directions of magnetic field-induced forces above magnets and experimentally observed
349 alignment of elongated macrophages is shown. Two characteristic locations were selected: the
350 first one above the maximum of the gradient lines between two magnets and the second one
351 close to the magnet corner, where two force components perpendicular to each other exist. These
352 forces are related to the magnets' edge-introduced gradients. Elongated macrophages were
353 observed along the maximum gradient lines and along a diagonal line very close to corners.

354 The cellular response to external mechanical stimuli results in several induced internal forces,
355 and such forces for the actin network are believed to be in the range of 10 pN to a few nN (30,
356 31). One other force is the adhesion force exerted by the cell to the substrate through focal
357 adhesion, and the magnitude of this force is in the range of 1-100 nN (32, 33). A single protein
358 stretching is reported to require 2-10 pN (34), whereas a single stress fiber stretching needs a
359 larger force of 10 nN (35, 36). High magnetic-field gradients interacting with diamagnetic
360 materials cause an effect analogous to microgravity (37-39) and produce forces of an order of
361 pN. Estimation of magnitude of such forces in our system is in the same range.

362 The nonhomogeneous magnetic field generated by our magnets was sufficiently high that
363 the resulting magnetic force applied to peritoneal mouse macrophages caused extreme
364 elongation (hummingbird phenotype) and acquisition of the anti-inflammatory M2
365 phenotype. This elongated M2-like phenotype mimics the phenotype resulting from the

366 pharmacological (Y27632 inhibitor) or genetic (macrophage-specific deletion of RhoA)
367 interference with the RhoA pathway (4-7). This suggests that application of a magnetic-field
368 gradient may potentially replace the RhoA interference approach to change macrophage
369 phenotype, functions and migration.

370 Although the elongated phenotype of RhoA-deleted and magnet-grown macrophages is
371 very similar, the mechanism of the extreme elongation in magnetic- versus RhoA-
372 interference seems to be different. In the RhoA interference situation, the elongated
373 macrophages permanently accumulated vinculin-rich focal adhesions in the tail, which
374 caused inability of the tail to detach from the substrate while the front of the macrophage
375 was moving forward (7). In contrast, the magnetic interference did not result in
376 accumulation of focal adhesions in the tail. Surprisingly, magnetic-field exposure caused
377 aggregation of vinculin in macrophage nuclei. It is known that the cell nucleus contains a
378 pool of nuclear actin that participates in regulation of chromatin status and gene
379 transcription. Thus, it is possible that magnet-induced changes in actin distribution affect not
380 only cytoplasmic but also nuclear actin and by doing so also influence actin-binding
381 molecules such as vinculin, causing its influx into the nucleus. In addition, the effect of a
382 magnetic field on macrophage Golgi differs from the effect of RhoA deletion. Magnetic
383 interference seems to cause dispersion of Golgi staining, while the RhoA-deletion highly
384 reduces Golgi staining. Thus, further studies are needed to establish what cytoskeletal
385 changes are responsible for extreme macrophage elongation during magnetic interference
386 and how they affect subcellular architecture and organelles.

387 Our preliminary hypothesis is that magnetic-field forces have changed the ionic currents
388 and/or distorted the macrophage membrane. Our preliminary results indicate that magnet-

389 exposed macrophages cluster the cation channel receptor TRPM2. Receptor clustering may
390 render it nonfunctional, which disrupts Ca^{+2} homeostasis. This, in turn, will affect actin
391 polymerization (which is ion current dependent) and lead to macrophage elongation. Similar
392 clustering of the CX3CR1 receptors (which direct macrophages to the transplanted organs) was
393 observed in RhoA-deleted macrophages) (4-7). Our previous studies showed that, under
394 control conditions, polarization of the M0 macrophage toward the M2 phenotype is
395 accompanied by macrophage elongation, which in turn induces an M2-specific gene-
396 expression pattern (4-7). This suggests that, when a macrophage is forced, by application of
397 a magnetic field, to elongate, it will switch on the expression of M2-specific genes such as
398 Arg-1.

399 We also observed that macrophages were aligned according to the magnetic forces'
400 pattern, as shown in Figures 10 and 11. We believe that the rotational magnetic-field forces,
401 due to high diamagnetic anisotropy of elongated macrophages, are responsible for such
402 behavior. In addition, we observed that macrophages were arranged in distinctive
403 rows/waves, in which macrophages closely followed each other. The wound-healing studies
404 showed that fibroblasts form the rows of cells with special "leader" cells that drag a
405 column of "follower" cells behind them (40, 41). These studies showed that the leader cell,
406 which is the first cell that had elongated, reorganized the actin cytoskeleton. These
407 cytoskeletal changes in the leader cell induced cytoskeletal changes and directional
408 movement of the followers. It is possible that a similar mechanism is responsible for the
409 creation of macrophage long rows/waves in response to the magnetic-field force.

410 The cellular cytoskeleton undergoes extensive rearrangements, not only in healthy cells
411 but also in cancer cells. The deregulation of cytoskeleton structure in many types of

412 human cancer is responsible for the increased divisions and migratory activity of tumor
413 cells and is linked with poor patient outcome. Thus, a magnetic field-initiated transduction
414 technique of introducing local mechanical forces on cells, while developed for macrophages
415 can be adapted and implemented for cancer cells.

416 Making the surrounding medium/tissue more paramagnetic can increase magnetic force acting
417 on cells. Magnetic resonance imaging contrast agents such as paramagnetic gadolinium can be
418 used to increase magnetic force on cells due to its paramagnetism (21). Correlation between
419 biochemical cell processes and cell deformation induced by forces generated by a magnetic-field
420 gradient will lead us to a better understanding of the magnetic-field interaction with the cells.

421

422 **ACKNOWLEDGMENTS**

423 The authors gratefully acknowledge support by the William Stamps Farish Fund, the Donald
424 D. Hammill Foundation, and the State of Texas through the Texas Center for Superconductivity
425 at the University of Houston. We also acknowledge very helpful conversations with Dmitri
426 Litvinov and Ivan Nekrashevich.

427 **AUTHOR CONTRIBUTIONS**

428 M.K. and J.W. designed research, analyzed data and wrote the paper; W.C. and K.Q.
429 conducted experiments, KQ also simulated magnetic field forces; RMG and JZK analyzed data.

430

431 **REFERENCES**

- 432 1. Mitchell RN (2009) Graft vascular disease: immune response meets the vessel wall. *Annu Rev*
433 *Pathol* 4:19-47.
- 434 2. Julius BK, *et al.* (2000) Incidence, progression and functional significance of cardiac allograft
435 vasculopathy after heart transplantation. *Transplantation* 69(5):847-853.
- 436 3. Nasr M, Sigdel T, & Sarwal M (2016) Advances in diagnostics for transplant rejection. *Expert*
437 *Rev Mol Diagn* 16(10):1121-1132.

- 438 4. Liu Y, *et al.* (2016) Mouse macrophage polarity and ROCK1 activity depend on RhoA and non-
439 apoptotic Caspase 3. *Exp Cell Res* 341(2):225-236.
- 440 5. Liu Y, *et al.* (2016) ROCK inhibition impedes macrophage polarity and functions. *Cell Immunol*
441 300:54-62.
- 442 6. Liu Y, *et al.* (2016) Dissonant response of M0/M2 and M1 bone-marrow-derived macrophages to
443 RhoA pathway interference. *Cell Tissue Res*.
- 444 7. Liu Y, *et al.* (2016) Macrophage/monocyte-specific deletion of Ras homolog gene family
445 member A (RhoA) downregulates fractalkine receptor and inhibits chronic rejection of mouse
446 cardiac allografts. *J Heart Lung Transplant*:30292-30293.
- 447 8. Ghibaud M, *et al.* (Substrate Topography Induces a Crossover from 2D to 3D Behavior in
448 Fibroblast Migration. *Biophysical Journal* 97(1):357-368.
- 449 9. Ladoux B & Nicolas A (2012) Physically based principles of cell adhesion mechanosensitivity in
450 tissues. *Reports on Progress in Physics* 75(11):116601.
- 451 10. Janmey PA (1998) The cytoskeleton and cell signaling: component localization and mechanical
452 coupling. *Physiol Rev* 78(3):763-781.
- 453 11. Liu J, Wang Y, Yuan X, Feng Y, & Liu H (2010) Cyclic-stretch induces the apoptosis of
454 myoblast by activation of Caspase-3 protease in a magnitude-dependent manner. *Int J Biochem*
455 *Cell Biol* 42(12):2004-2011.
- 456 12. Oh S, Kwon D, Lee HJ, Kim J, & Lee E (2010) Role of elevated pressure in TRAIL-induced
457 apoptosis in human lung carcinoma cells. *Apoptosis* 15(12):1517-1528.
- 458 13. Boccafoschi F, Sabbatini M, Bosetti M, & Cannas M (2010) Overstressed mechanical stretching
459 activates survival and apoptotic signals in fibroblasts. *Cells Tissues Organs* 192(3):167-176.
- 460 14. Miyakoshi J (2005) Effects of static magnetic fields at the cellular level. *Prog Biophys Mol Biol*
461 87(2-3):213-223.
- 462 15. Murabayashi S (2013) Application of magnetic field for biological response modification.
463 *Biomed Mater Eng* 23(1-2):117-128.
- 464 16. Valiron O, *et al.* (2005) Cellular disorders induced by high magnetic fields. *Journal of Magnetic*
465 *Resonance Imaging* 22(3):334-340.
- 466 17. Qian A-R, *et al.* (2013) Large gradient high magnetic fields affect osteoblast ultrastructure and
467 function by disrupting collagen I or fibronectin/ $\alpha\beta 1$ integrin. *PLoS one* 8(1):e51036.
- 468 18. Shi D, *et al.* (2010) Effects of microgravity modeled by large gradient high magnetic field on the
469 osteogenic initiation of human mesenchymal stem cells. *Stem Cell Reviews and Reports* 6(4):567-
470 578.
- 471 19. Kauffmann P, *et al.* (2011) Diamagnetically trapped arrays of living cells above micromagnets.
472 *Lab Chip* 11(18):3153-3161.
- 473 20. Denegre JM, Valles JM, Jr., Lin K, Jordan WB, & Mowry KL (1998) Cleavage planes in frog
474 eggs are altered by strong magnetic fields. *Proc Natl Acad Sci U S A* 95(25):14729-14732.
- 475 21. Winkleman A, *et al.* (2004) A magnetic trap for living cells suspended in a paramagnetic buffer.
476 *Applied physics letters* 85(12):2411-2413.
- 477 22. Zablotskii V, *et al.* (2013) Life on magnets: stem cell networking on micro-magnet arrays. *PLoS*
478 *One* 8(8):e70416.
- 479 23. Multiphysics C (2007) User's guide. *Version 4*:290-298.
- 480 24. Zablotskii V, *et al.* (2010) High-Field Gradient Permanent Micromagnets for Targeted Drug
481 Delivery with Magnetic Nanoparticles. 152-157.
- 482 25. Kashio M, *et al.* (2012) Redox signal-mediated sensitization of transient receptor potential
483 melastatin 2 (TRPM2) to temperature affects macrophage functions. *Proc Natl Acad Sci U S A*
484 109(17):6745-6750.
- 485 26. Beceiro S, *et al.* (2017) TRPM2 ion channels regulate macrophage polarization and gastric
486 inflammation during *Helicobacter pylori* infection. *Mucosal Immunol* 10(2):493-507.
- 487 27. Chionna A, *et al.* (2003) Cell shape and plasma membrane alterations after static magnetic fields
488 exposure. *Eur J Histochem* 47(4):299-308.

- 489 28. Gassner AL, *et al.* (2009) Magnetic forces produced by rectangular permanent magnets in static
490 microsystems. *Lab Chip* 9(16):2356-2363.
- 491 29. Eguchi Y, Ueno S, Kaito C, Sekimizu K, & Shiokawa K (2006) Cleavage and survival of
492 *Xenopus* embryos exposed to 8 T static magnetic fields in a rotating clinostat.
493 *Bioelectromagnetics* 27(4):307-313.
- 494 30. Giardini PA, Fletcher DA, & Theriot JA (2003) Compression forces generated by actin comet
495 tails on lipid vesicles. *Proceedings of the National Academy of Sciences* 100(11):6493-6498.
- 496 31. Noireaux V, *et al.* (Growing an Actin Gel on Spherical Surfaces. *Biophysical Journal* 78(3):1643-
497 1654.
- 498 32. Balaban NQ, *et al.* (2001) Force and focal adhesion assembly: a close relationship studied using
499 elastic micropatterned substrates. *Nature cell biology* 3(5):466-472.
- 500 33. Stricker J, Aratyn-Schaus Y, Oakes Patrick W, & Gardel Margaret L (Spatiotemporal Constraints
501 on the Force-Dependent Growth of Focal Adhesions. *Biophysical Journal* 100(12):2883-2893.
- 502 34. Grashoff C, *et al.* (2010) Measuring mechanical tension across vinculin reveals regulation of
503 focal adhesion dynamics. *Nature* 466(7303):263-266.
- 504 35. Deguchi S, Ohashi T, & Sato M (Tensile properties of single stress fibers isolated from cultured
505 vascular smooth muscle cells. *Journal of Biomechanics* 39(14):2603-2610.
- 506 36. Zablotskii V, *et al.* (2016) Effects of high-gradient magnetic fields on living cell machinery.
507 *Journal of Physics D: Applied Physics* 49(49):493003.
- 508 37. Beaugnon E & Tournier R (1991) Levitation of organic materials. *Nature* 349(6309).
- 509 38. Kuznetsov OA & Hasenstein KH (1996) Intracellular magnetophoresis of amyloplasts and
510 induction of root curvature. *Planta* 198(1):87-94.
- 511 39. Yamaguchi M & Tanimoto Y (2006) Magneto-Science. *Magneto-Science: Magnetic Field Effects*
512 *on Materials: Fundamentals and Applications, Springer Series in Materials Science, Volume 89.*
513 *ISBN 978-3-540-37061-1. Kodansha Ltd. and Springer-Verlag Berlin Heidelberg, 2006 1.*
- 514 40. Omelchenko T, Vasiliev JM, Gelfand IM, Feder HH, & Bonder EM (2003) Rho-dependent
515 formation of epithelial "leader" cells during wound healing. *Proc Natl Acad Sci U S A*
516 100(19):10788-10793.
- 517 41. Gov NS (2007) Collective cell migration patterns: follow the leader. *Proc Natl Acad Sci U S A*
518 104(41):15970-15971.
- 519

520 **Figure Legends:**

521 **Figure 1. Magnetic field and magnetic field-induced mechanical force patterns.**

522 (A) Theoretically calculated magnetic induction vector component B_z in the YZ plane; (B) magnetic-
523 induction magnitude in the YZ plane; (C) magnetic-field gradient (∇B_z) contour projection in the YZ
524 plane; (D) mechanical force acting on a cell along the Y-axis are shown for 2 very closely aligned
525 together, 5-mm wide, 10-mm long, and 1.9-mm-thick, magnets configured in an opposite magnetic
526 polarization (NS-SN) directions.

527 **Figure 2. Experimental setup.**

528 A sketch describing an experimental configuration of two permanent magnets covered by a very thin
529 glass plate is presented. Three of the most characteristic areas above the magnets, where highly elongated
530 and magnetic-field unaffected macrophages were present, are marked as #1, #2 and #3 rectangular shapes,
531 respectively. #1 refers to the interface where the maximum of the gradient was created, #2 marks an area
532 close to the magnet corners along the diagonal line of the whole structure. #3 marks an area outside of the
533 magnetic field. A calculated distribution of the magnetic field-induced force component present above the
534 magnets is also included here.

535

536 **Figure 3. Distribution and phenotype of macrophages on magnets.**

537 Distribution and phenotype of M0 macrophages grown on control (A, B) and magnet (C, D, E) slides
538 are shown. Macrophage actin is stained with rhodamine-phalloidin (red). Macrophages grown on slides
539 without a magnetic field applied exhibit roundish or only slightly elongated shapes (A, B). Grown-on-
540 magnets macrophages are significantly elongated, some with an unusually thin tail and overall length
541 $>150\ \mu\text{m}$ (E). In addition, macrophages grown on magnets are arranged in rows or “waves” with a
542 crisscrossing pattern and mostly aligned toward the corners of the magnets (C, D). The bar is equal to 500
543 μm in A, C, D; 200 μm in B and 100 μm in E. The (F) graph shows comparison between the number of
544 elongated cells within 2mm^2 areas within the rows of elongated cells on the magnets (from 5 different
545 magnets) and the number of elongated cells in the areas without the magnet. The difference in elongation
546 with and without the magnet is highly statistically significant ($P=0.0012$).

547

548 **Figure 4. Hummingbird phenotype of magnet-exposed and RhoA-deleted macrophages.**

549 Macrophages stained with rhodamine-phalloidin (red) to visualize actin. (A) Graph shows that the
550 average length of elongated magnet-exposed and RhoA-deleted macrophages (grown without magnets) is
551 very similar; the length differences are statistically nonsignificant ($P=0.8425$). Control macrophage (B) is
552 slightly elongated, while magnet- grown (C) and RhoA-deleted, grown without magnets (D) macrophages

553 are extremely elongated, acquiring a hummingbird phenotype. Nuclei are stained with DAPI (blue).
554 Panels B-D are merged images of actin and DAPI staining. Bar is equal to 100 μm

555

556 **Figure 5. Vinculin distribution in macrophages.**

557 Actin (red) and vinculin (green) staining of control (A-C), RhoA-deleted (D, E) and magnet-exposed
558 (F-I) macrophages. Macrophages grown on control slides are slightly elongated with clearly visible
559 podosomes (short arrows) and focal adhesion protein vinculin distributed around the nuclei and in the
560 podosome area (A-C)). RhoA-deleted macrophages (D, E) show podosomes, vinculin in the tail (long
561 arrows) and in the podosome area, and lack of vinculin in the nucleus. Macrophages grown on magnets
562 (F-I) are extremely elongated, and vinculin is present in the nuclei (H, I). DAPI-stained nuclei (N) are
563 blue. Panels B and C are merged images of actin and DAPI staining. Panel E is a merged image of
564 vinculin and DAPI staining. Panel H is a merged image of actin and vinculin staining. Bar is equal to 50
565 μm

566

567 **Figure 6. Golgi complex distribution in control, magnet-grown and RhoA-deleted**
568 **macrophages.**

569 In control macrophages (A) the Golgi complex (arrows) is in the vicinity of the nucleus. In contrast,
570 magnet-grown macrophages (B) do not have any visible Golgi complex and show GM130-positive
571 staining dispersed in the cytoplasm (arrows). In RhoA-deleted macrophages (C) the remnants of the Golgi
572 complex (arrow) are in the vicinity of the nucleus. Nuclei are stained with DAPI (blue). All panels are
573 merged images of DAPI and GM130 staining. Bar in A, C is equal to 100 μm and in B to 50 μm .

574

575 **Figure 7. Macrophage markers expression.**

576 Western blot analysis of M1 (inflammatory) and M2 (anti-inflammatory) markers' expression with anti-
577 iNOS and anti-Arg-1 antibodies. The control and magnet-grown (Mag 1, Mag 2) M0 macrophages did not

578 express the M1 marker iNOS protein, and the expression of the M2 marker Arg-1 was highly upregulated
579 in magnet-grown M0 macrophages. GAPDH was used as a loading marker. The upper panel is one
580 example of a Western blot from a single experiment, and the lower panel presents a graph of GAPDH to
581 Arg-1 ratio values from 3 independent experiments. Mag 1 and Mag 2 are two independent magnet
582 configuration settings. The p value is equal to 0.0584.

583

584 **Figure 8. TRPM2 distribution in macrophages.**

585 Macrophages were stained with rhodamine-phalloidin (red) for actin and with anti-TRPM2 antibody
586 and FITC-conjugated secondary antibody (green). Nuclei were stained with DAPI (blue). (A, B) The
587 control macrophage shows uniform distribution of TRPM2 (arrows) in the cytoplasm of the macrophage
588 body and tail. (C, D) In macrophages exposed to the magnetic-field gradient, the TRPM2 is clustered
589 around the nucleus (arrows) and absent in the tail. Panels A, C are merged images of actin and DAPI
590 staining. Panels B, D are merged images of DAPI and TRPM2 staining. Bar is equal to 50 μ m.

591

592 **Figure 9. The summary of magnet and RhoA-deletion effects on actin and actin-related structures**
593 **in the M0 macrophages.**

594 Diagram of actin and actin-dependent structure changes caused by magnetic-field exposure in
595 comparison to the changes in RhoA-deleted macrophages. The control macrophage is slightly
596 elongated, with the Golgi complex situated in the vicinity of the nucleus. Vinculin-rich focal
597 adhesions and CX3CR1 and TRPM2 receptors are distributed at the cell membrane. Macrophage-
598 specific deletion of RhoA causes disruption of actin, macrophage elongation, disruption of Golgi
599 and aggregation of the CX3CR1 receptors and the localization of focal adhesions in the
600 macrophage tail (4-7). Macrophage exposure to a magnetic field causes actin disruption,
601 macrophage elongation, disruption of Golgi and aggregation of the TRPM2 receptor. However,

602 in contrast to the RhoA-deleted macrophages, there is no noticeable aggregation of focal
603 adhesions in the tail, and vinculin translocates to the nuclei.

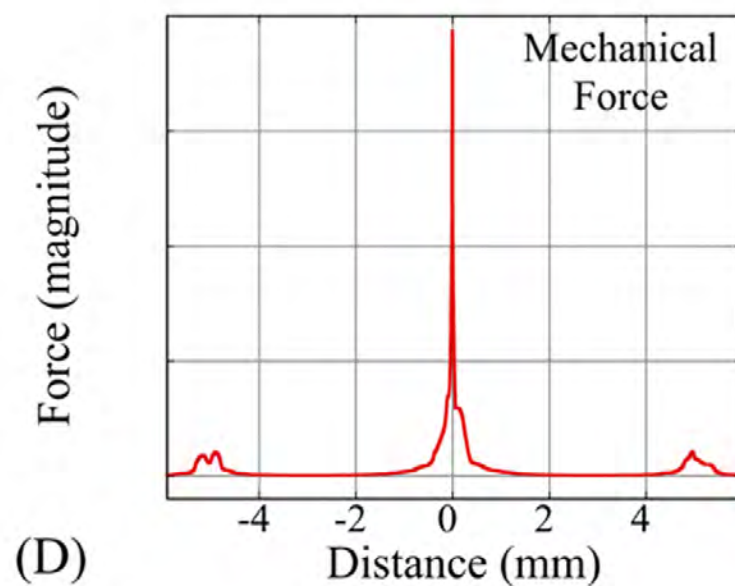
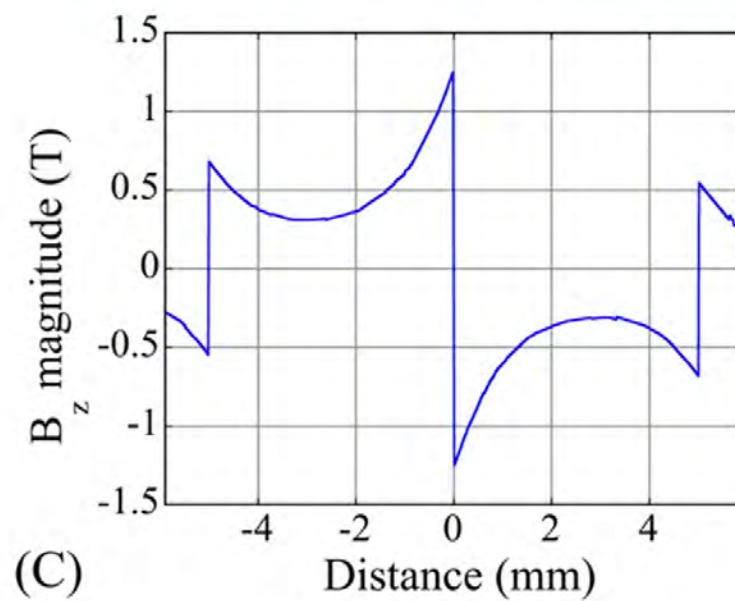
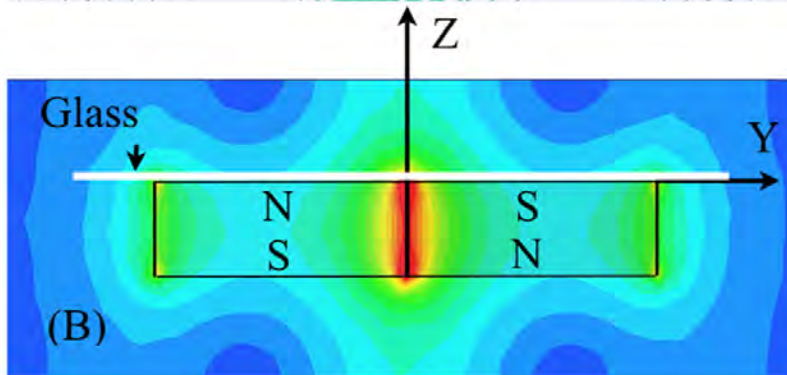
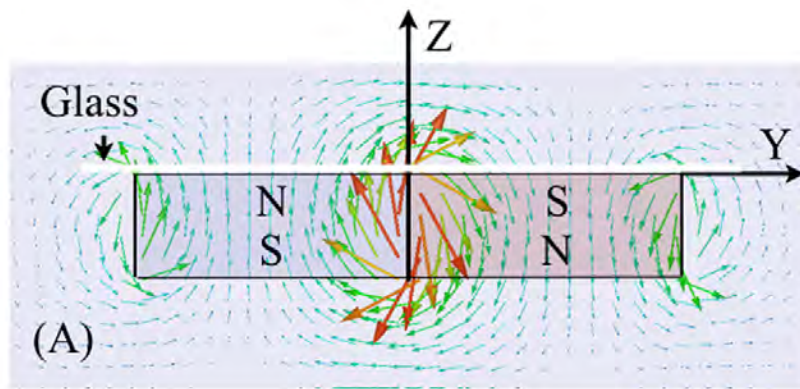
604

605 **Figure 10. Cell with magnetic field interaction**

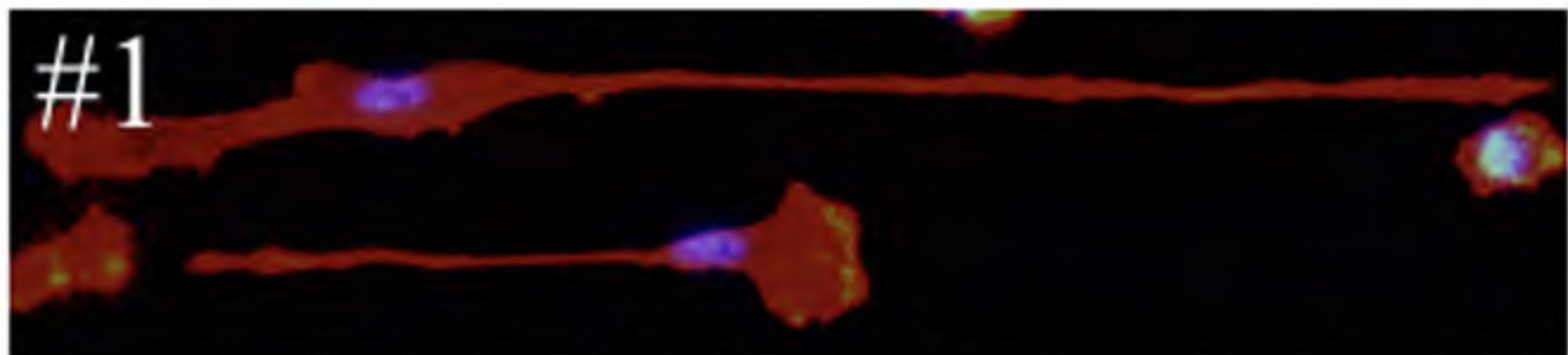
606 Two examples of possible forces exerted due to the presence of magnetic field. (A) The Lorentz force
607 acting on a membrane calcium channel (magnetic-field interaction with ions' currents) is depicted. (B)
608 The second force (susceptibility buoyance) acting, in the presence of a nonuniform magnetic field, on a
609 diamagnetic cell in less diamagnetic buffer is shown. This is an experimentally observed case, and the
610 cells are attracted to the highest-gradient area.

611

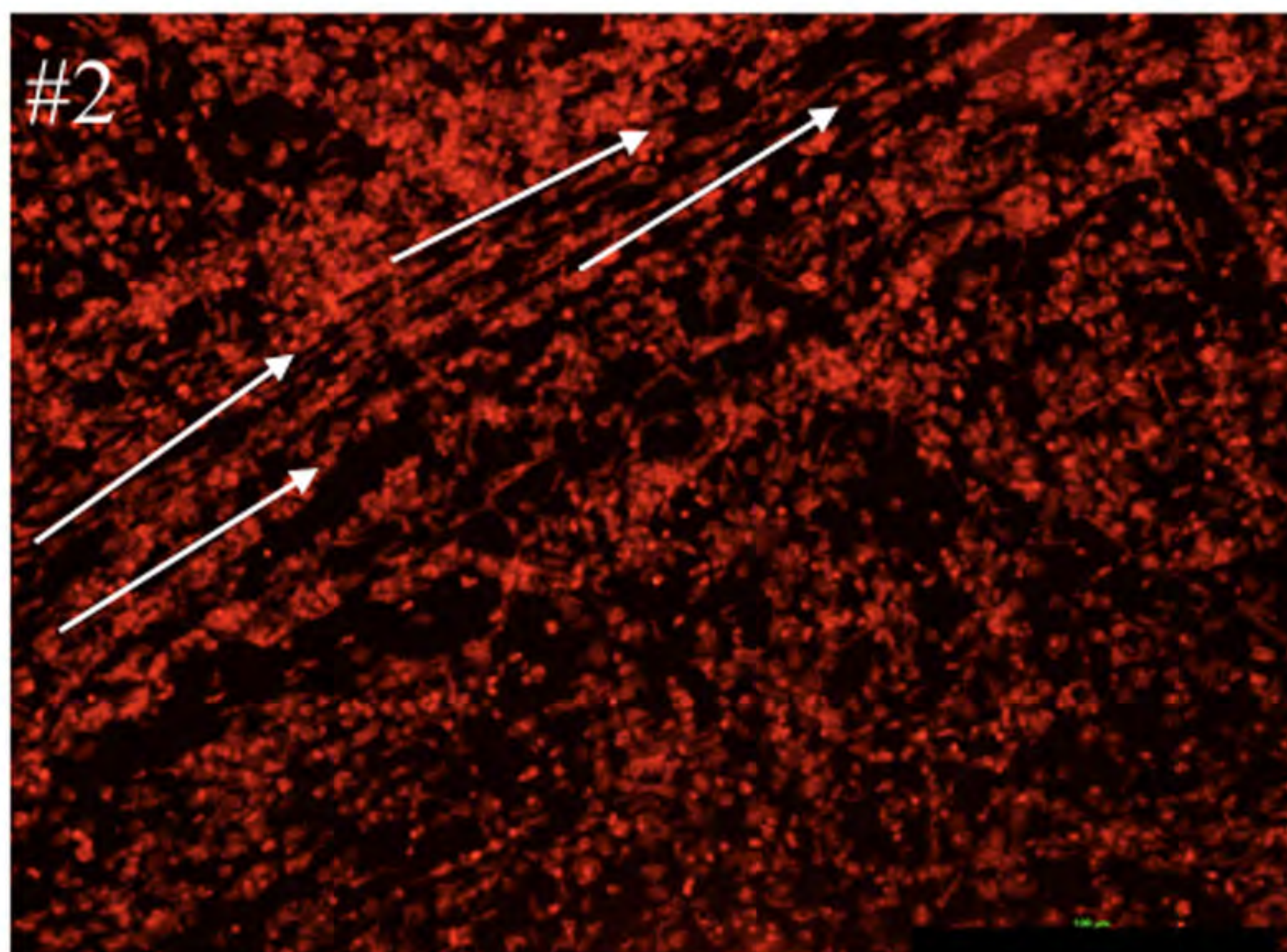
612 **Figure 11. Magnetic field-induced mechanical force patterns and observed elongated**
613 **macrophages' location and alignment.** Magnetic-force mapping (projection of the force into the XY-
614 plane) is shown (blue color indicates the weakest force magnitude). Enlargements show the magnetic
615 field force distribution at the magnet corner and at the magnets' interface in the XY plane. At the
616 interface the elongated macrophages are aligned mostly in a perpendicular direction to the magnetic
617 gradient-generated force vectors. Whereas close to the corner long-range, well-aligned macrophages,
618 grouped along the diagonal of both magnets, can be seen. Macrophages in this area are subjected to two
619 magnetic field (nonuniform)-generated forces perpendicular to each other.



Magnetic field gradient plot along y-axis

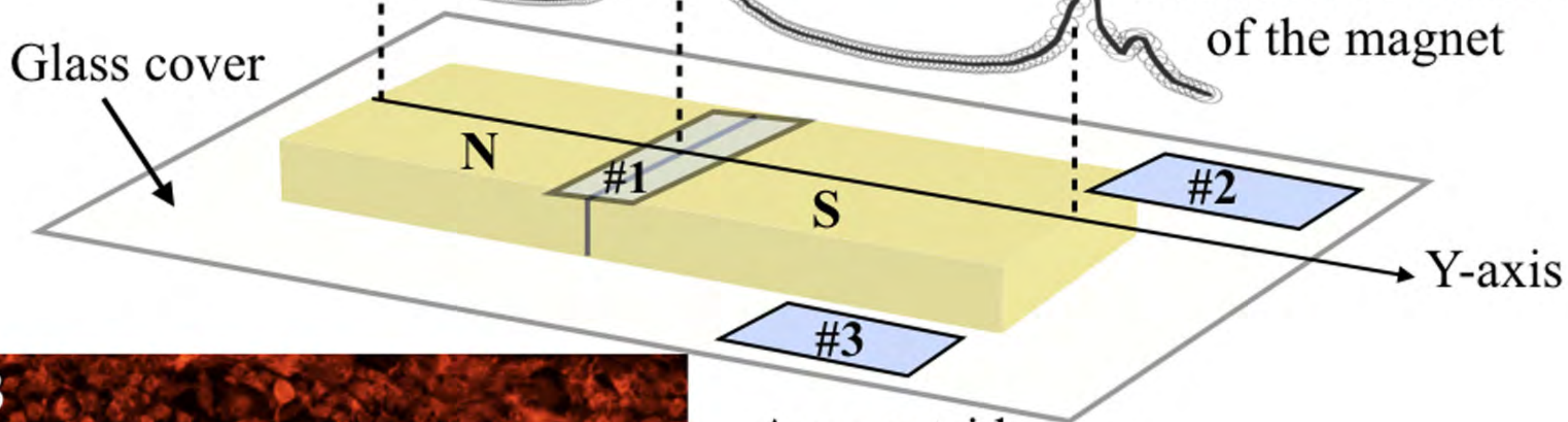


Area of maximum gradient field

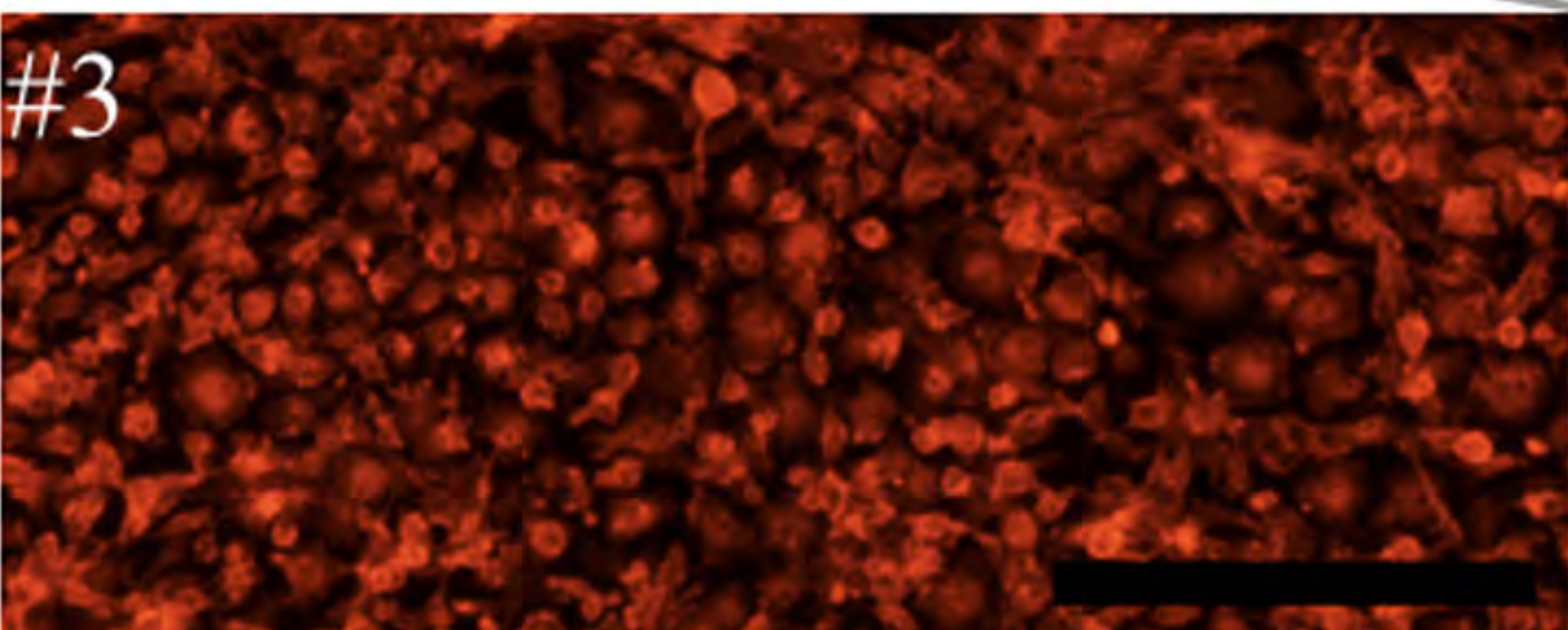


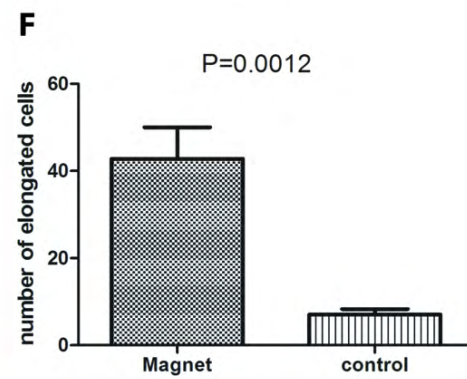
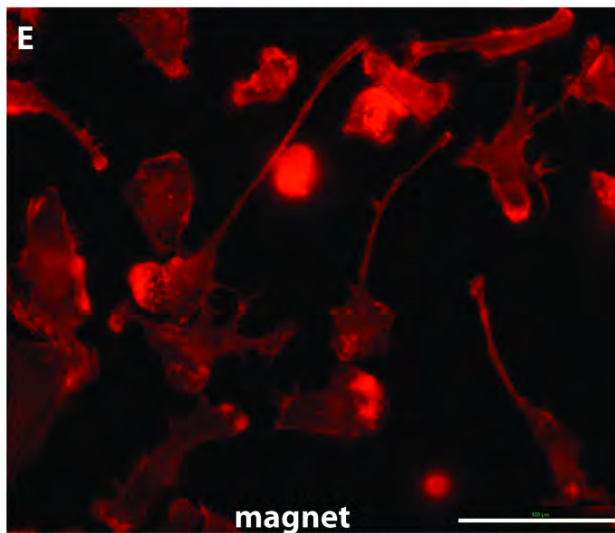
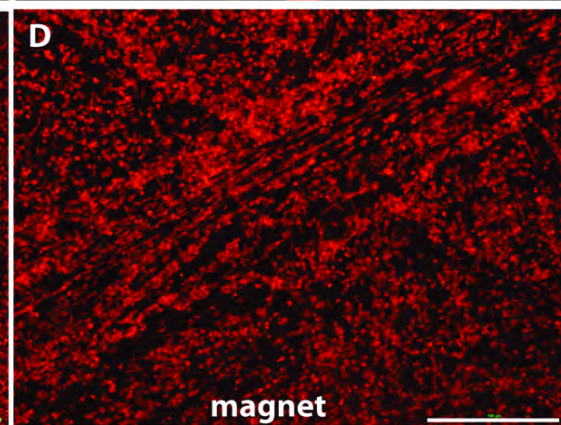
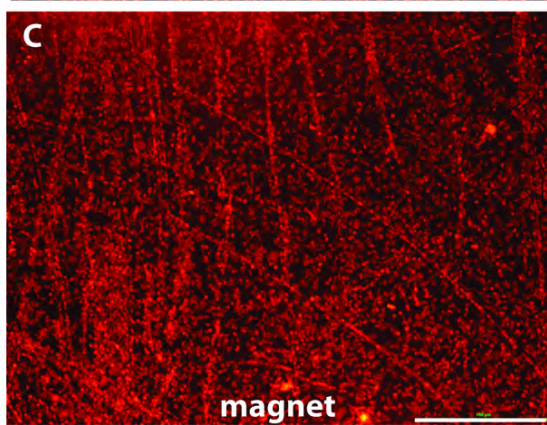
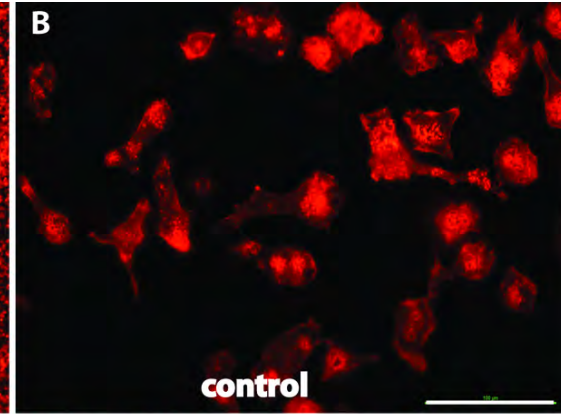
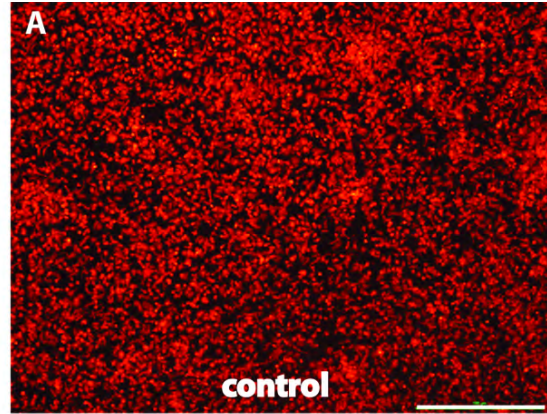
Area close to corner of the magnet

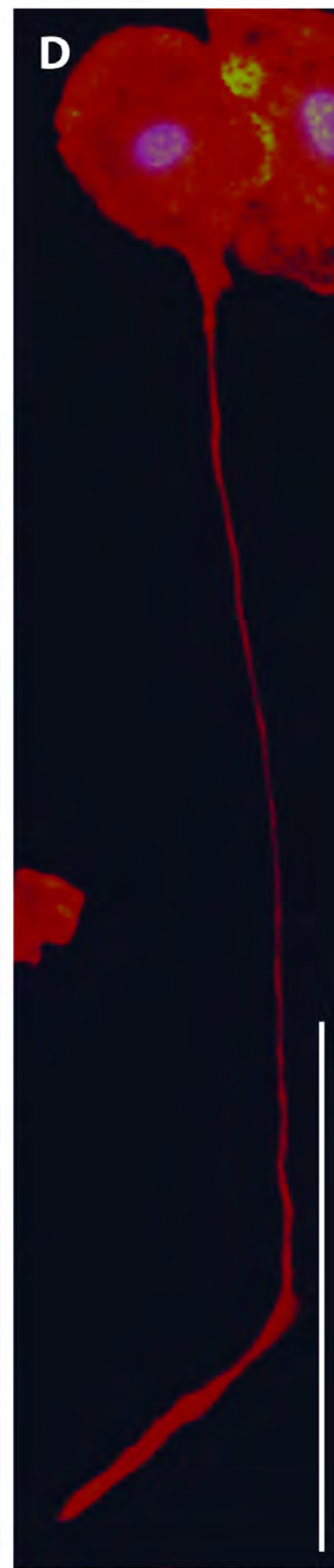
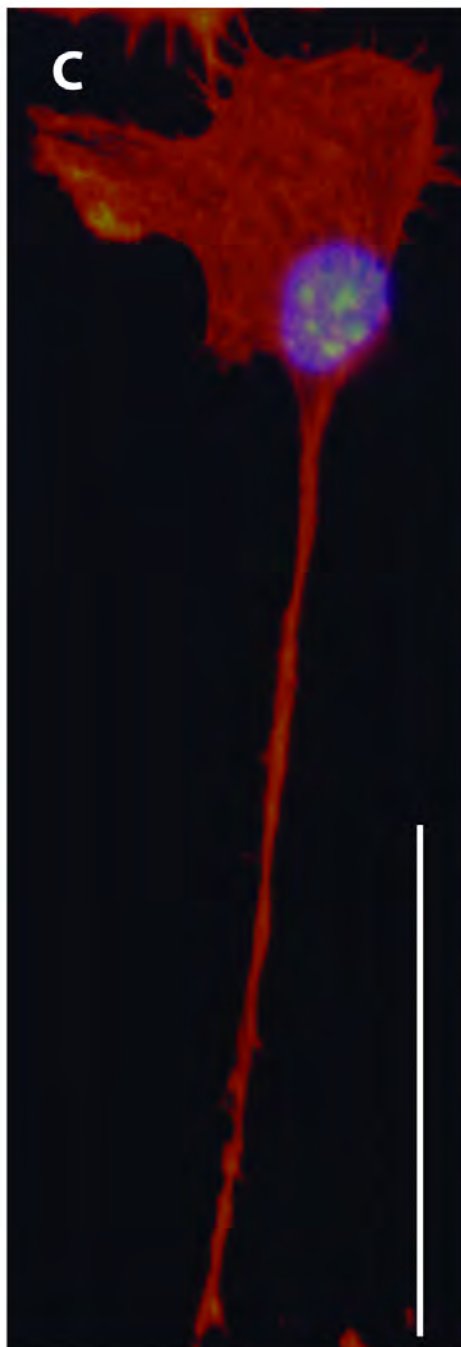
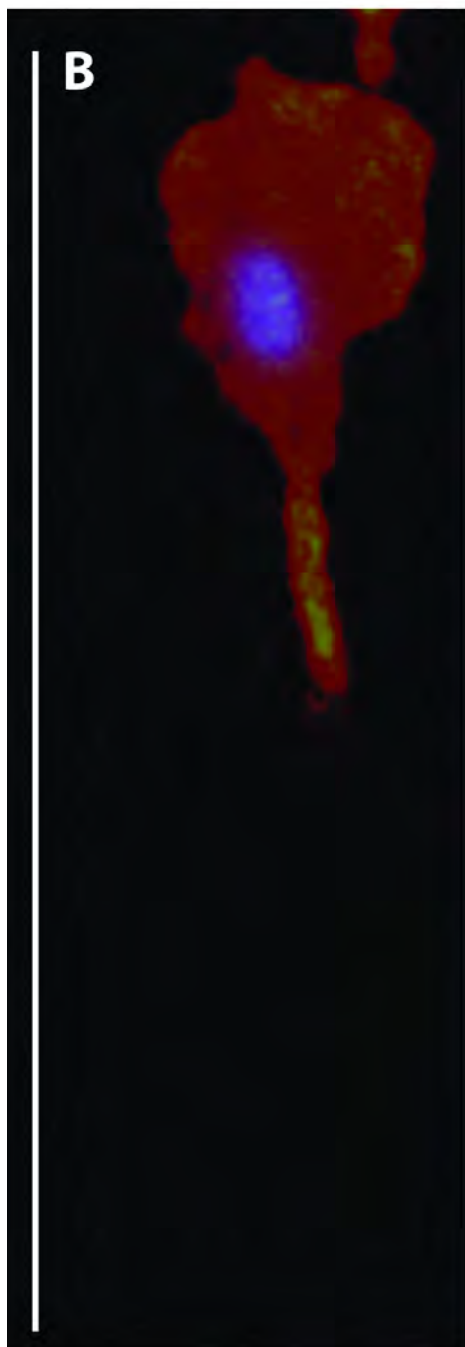
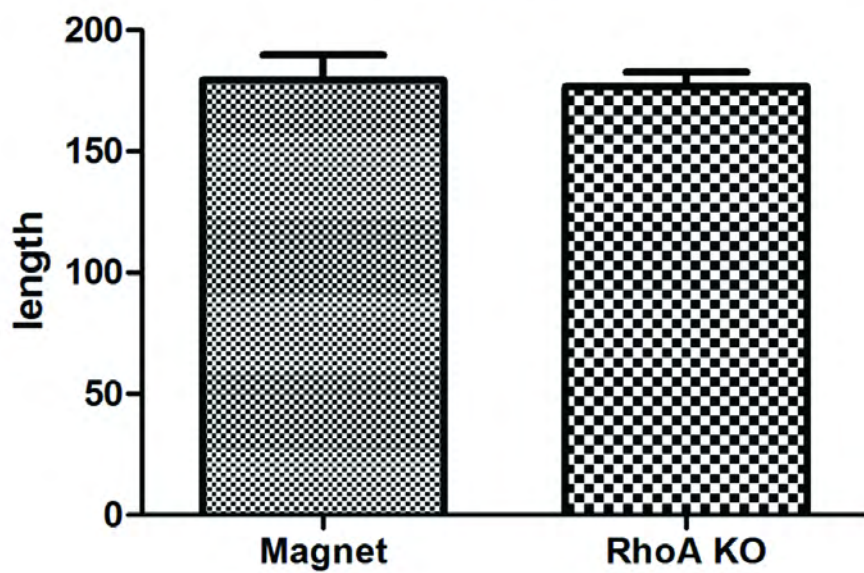
Glass cover

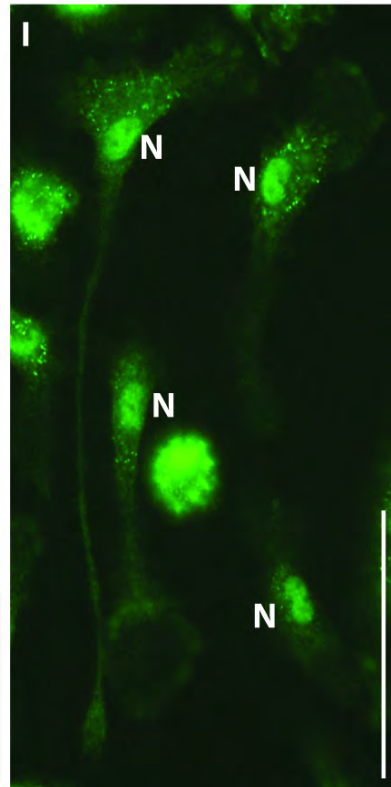
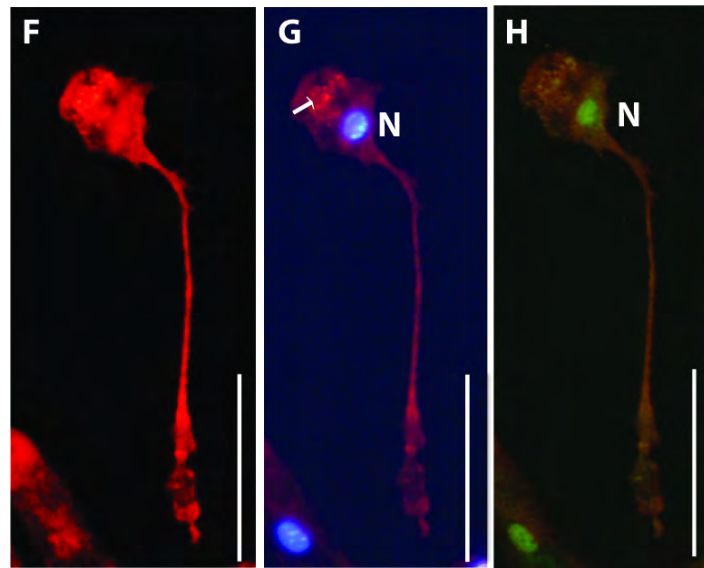
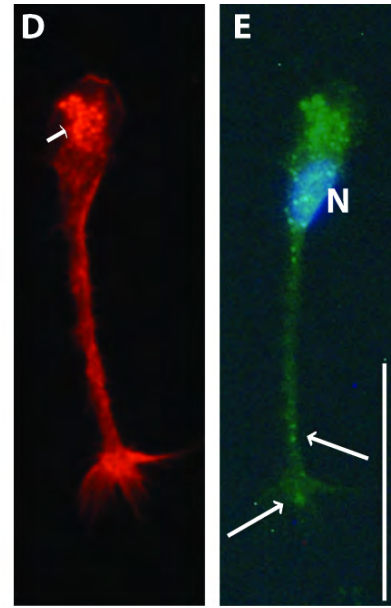
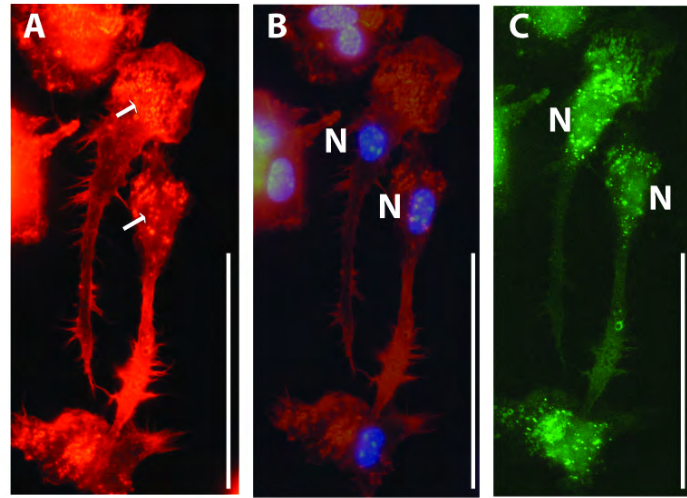


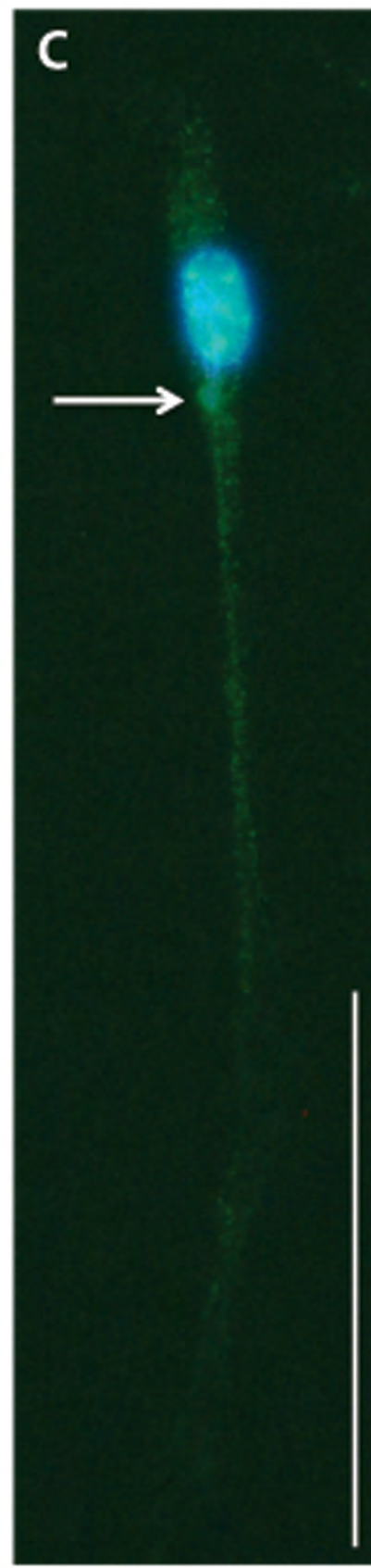
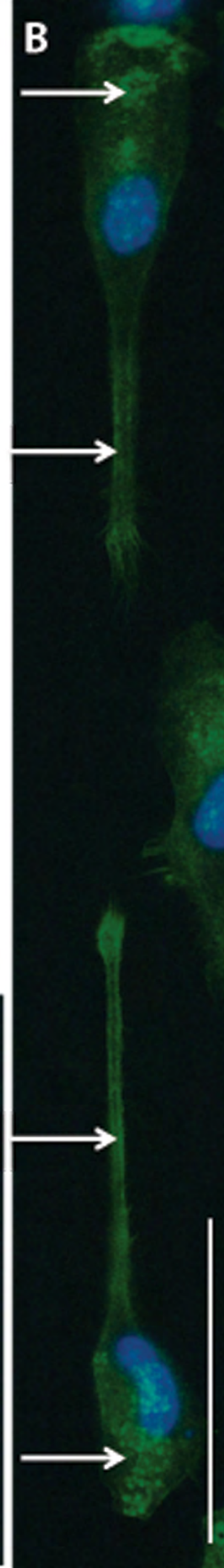
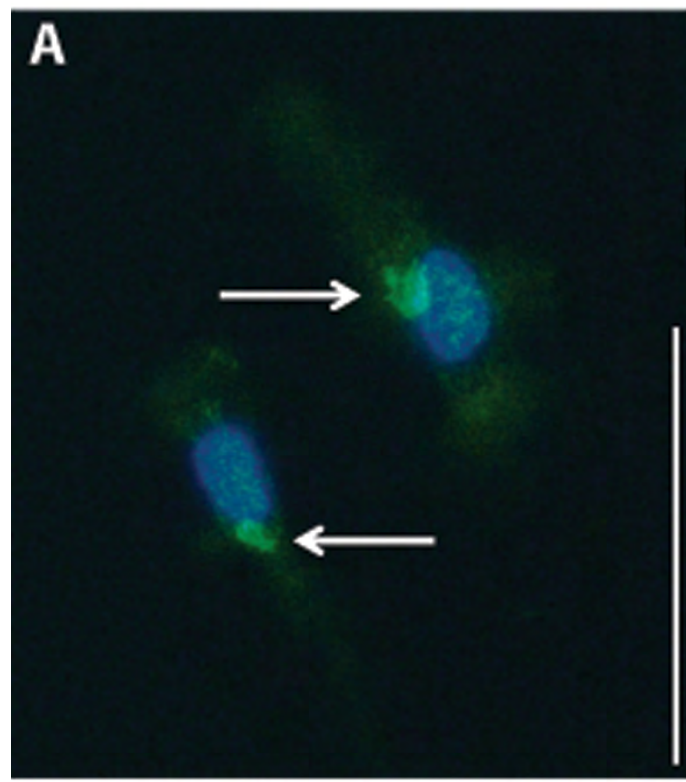
Area outside of magnetic field interaction

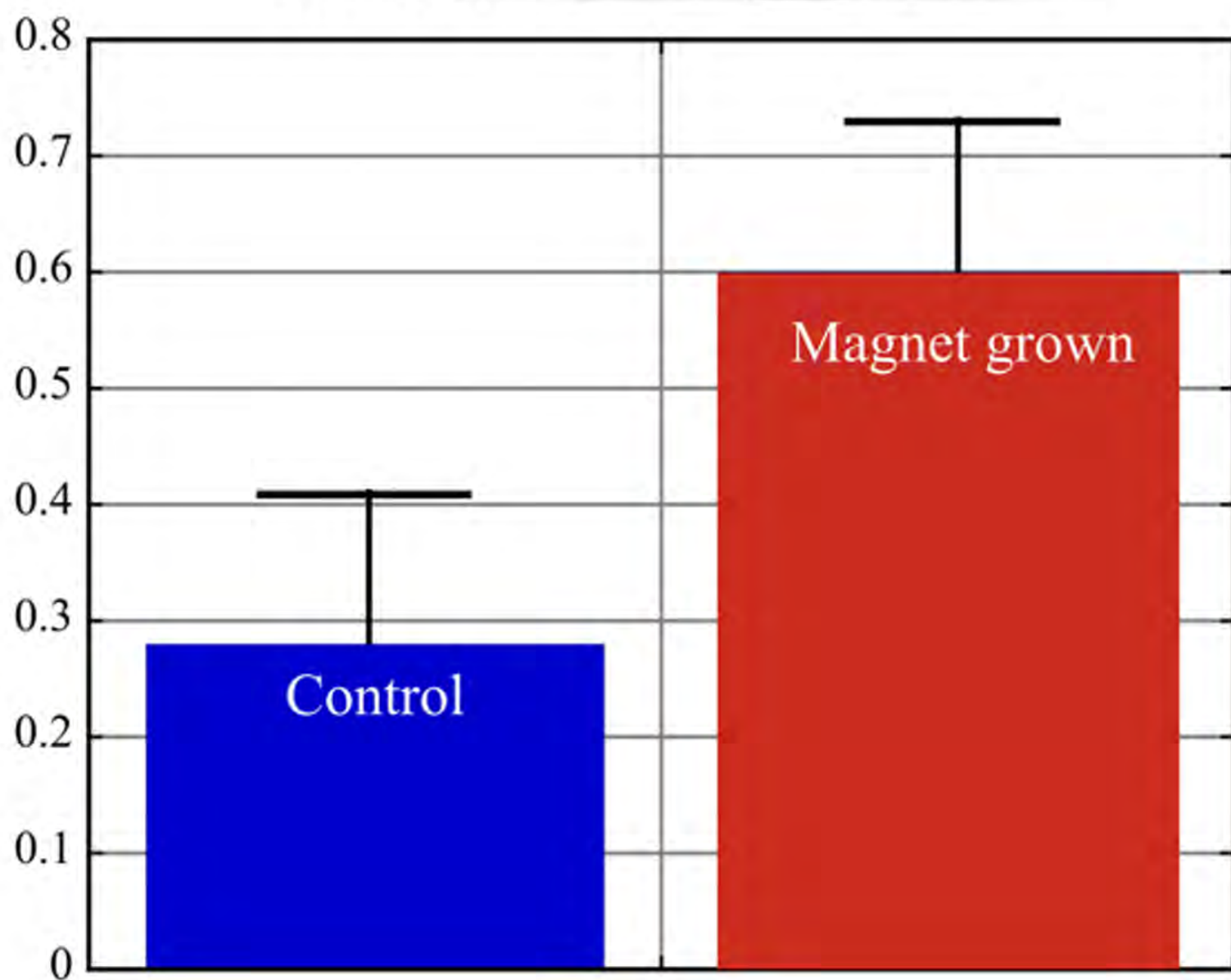
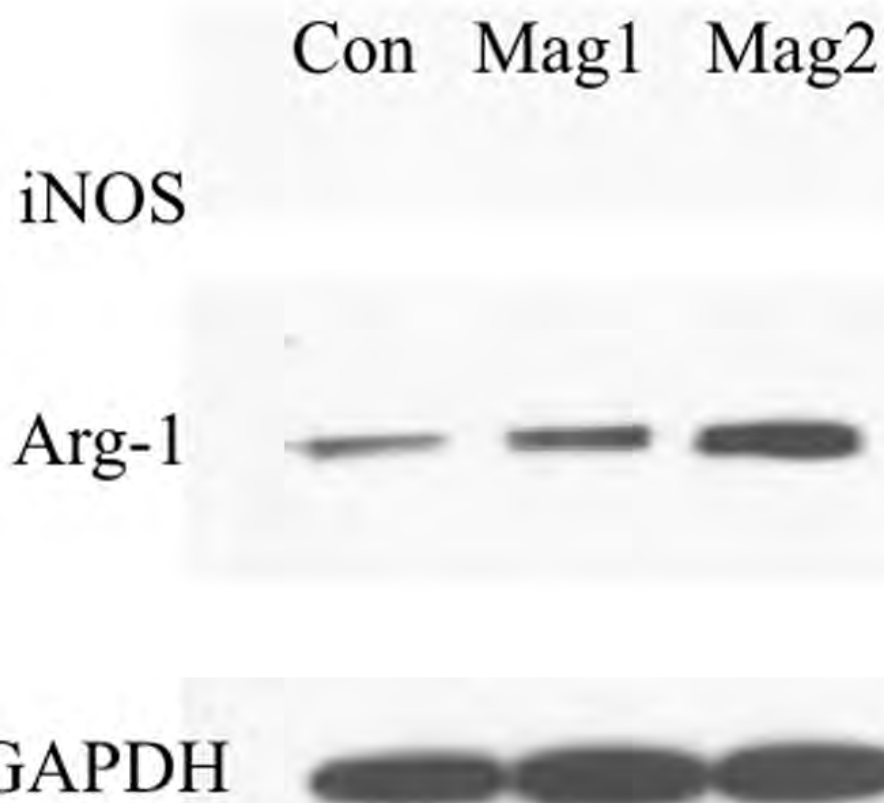


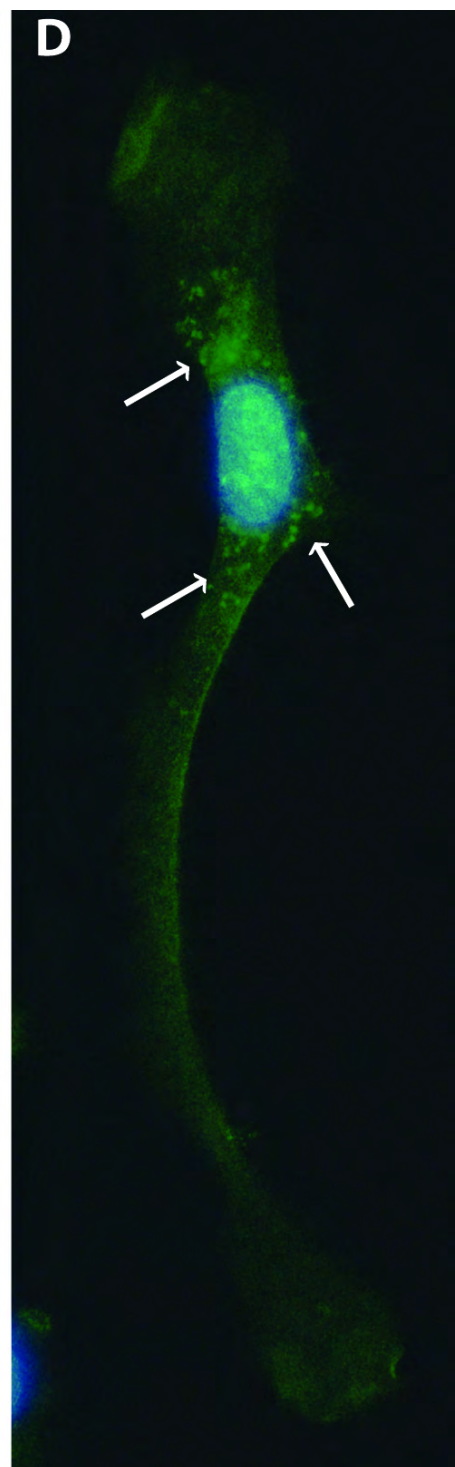
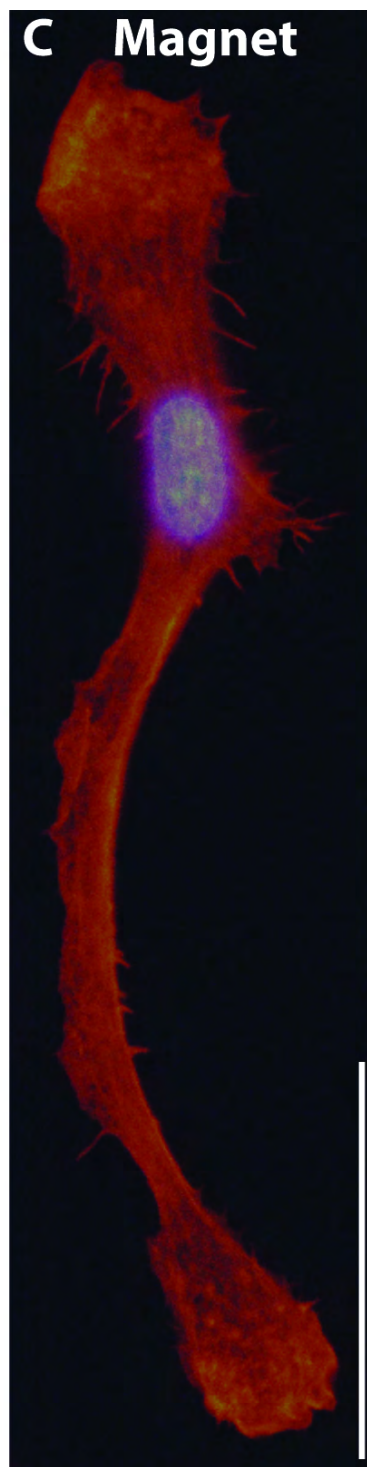
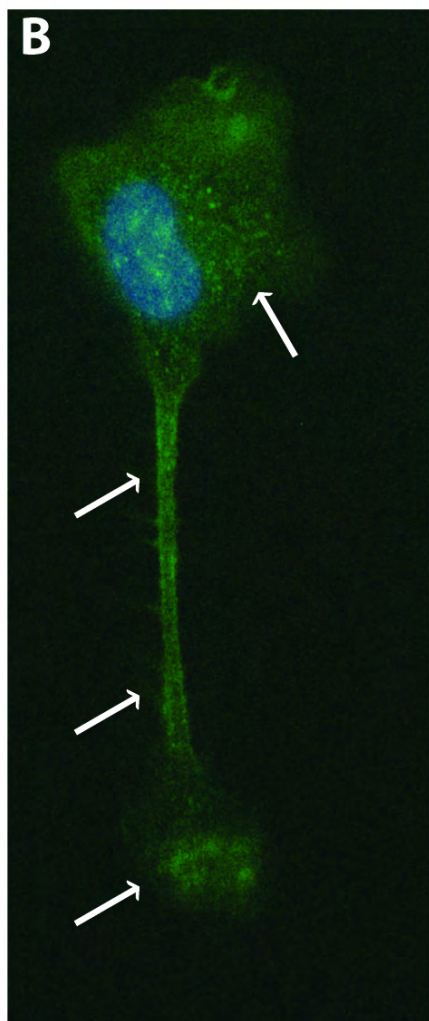
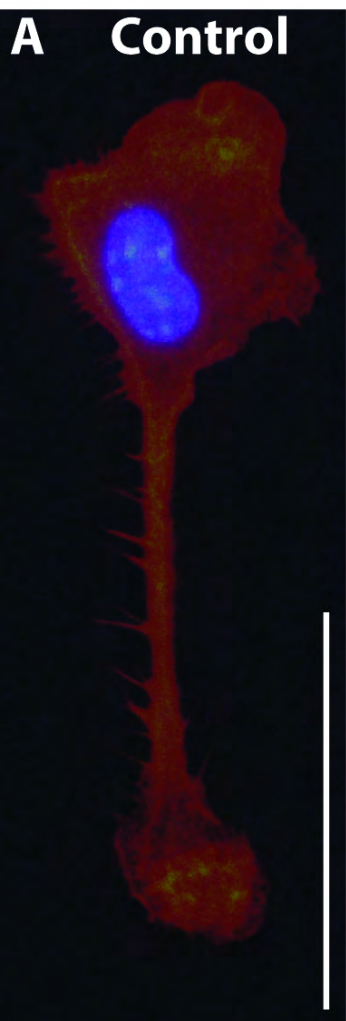


A $P=0.8425$ 

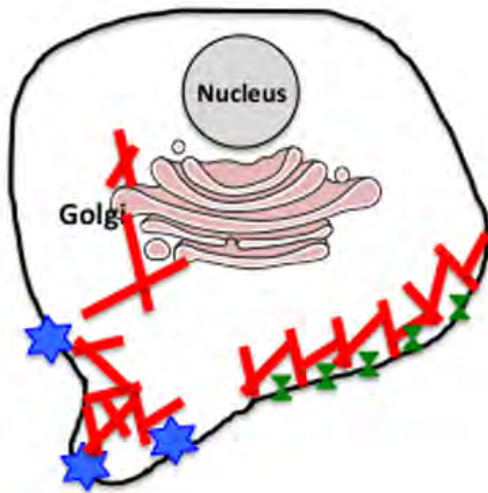




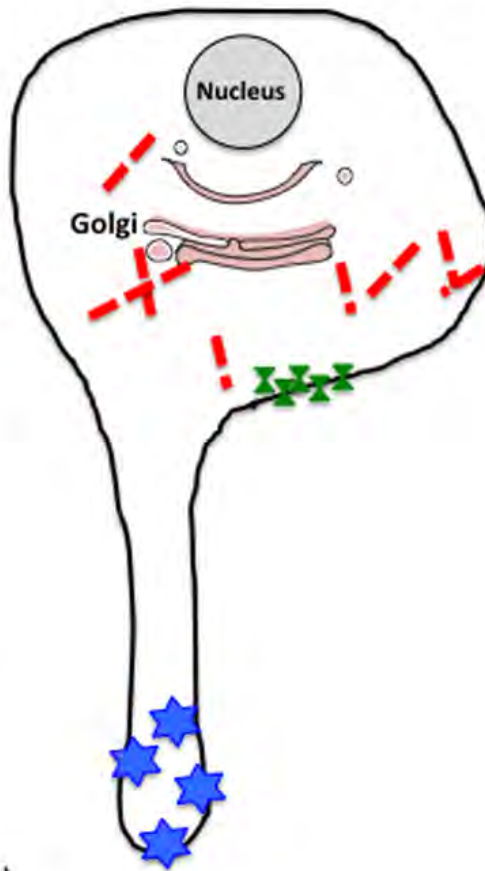




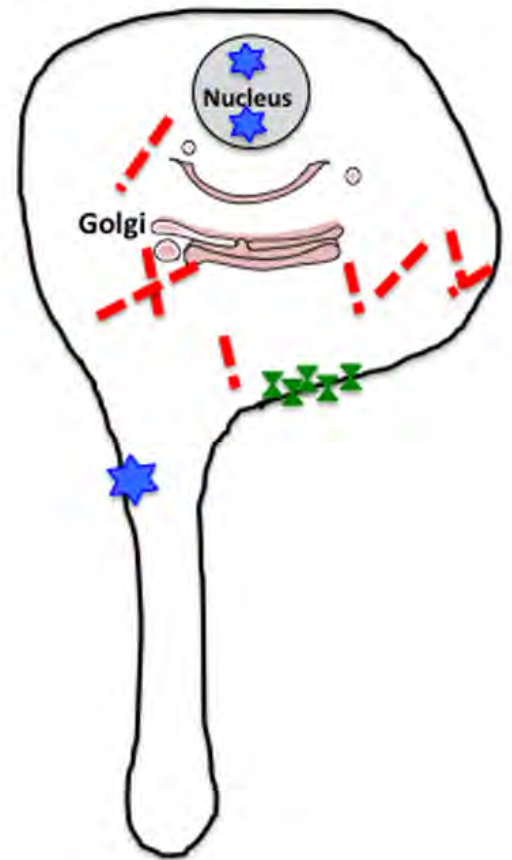
Control macrophage



RhoA-deleted macrophage



Magnet-exposed macrophage



-  actin
-  disrupted actin
-  receptor
-  Vinculin
Focal adhesions (FAs)

